PERGAMON

International Journal of Solids and Structures 39 (2002) 3199–3216

INTERNATIONAL JOURNAL OF SOLIDS and STRUCTURES

www.elsevier.com/locate/ijsolstr

Modeling of femtosecond laser-induced non-equilibrium deformation in metal films

J.K. Chen [a,*], J.E. Beraun [a], L.E. Grimes [a], D.Y. Tzou [b]

[a] *Laser Effects Research Branch, Directed Energy Directorate, Air Force Research Laboratory, Kirtland AFB, NM 87117, USA*
[b] *Department of Mechanical and Aerospace Engineering, University of Missouri-Columbia, Columbia, MO 65211, USA*

Received 15 July 2001; received in revised form 5 March 2002

Abstract

This paper extends the dual-hyperbolic two temperature (Numer. Heat Transfer Part A 40 (2001) 1) and hot-electron blast (J. Exp. Theor. Phys. 88 (1999) 84) models to investigate the deformation in metal films subjected to ultrashort laser heating. A new set of fully coupled, transient thermoelasticity equations is derived based on the assumption of uniaxial strain but three-dimensional stress. Two potential material removal mechanisms, thermal (melting) and non-thermal (high stress), are identified. Numerical results show that the non-thermal damage could be a dominating mechanism in ultrashort laser-material ablation. The major driving force for the non-thermal damage is the so-called hot-electron blast force, which is generated by non-equilibrium hot electrons. It is also found that for gold films thicker than 200 nm, a thin layer of material near the heated surface could be removed, as experimentally observed (Opt. Cummun. 129 (1996) 134; J. Appl. Phys. 85 (1999) 6803). On the other hand, damage could initiate from the middle region and then extend over the entire film for a gold film of 50 nm in thickness or thinner.

Keywords: Femtosecond lasers; Ultrashort laser-material ablation; Ultrafast thermomechanics; Two-step heating process; Hot-electron blast force; Metal films; Non-thermal damage

1. Introduction

Ultrashort (femtoseconds to a few picoseconds) laser pulses can now generate optical peak powers as high as petawatts with frequencies spanning from X-rays to T-rays (terahertz radiation). Due to the intense, micro-scale heating in such an extremely short period of time, interactions of an ultrashort laser beam with solid matter have demonstrated advantages over conventional lasers in physics, chemistry and biology. For example, ultrashort lasers have a unique capability of very high precision control with minimal collateral damage (Momma et al., 1996; Perry et al., 1999). Moreover, they can ablate practically any material with a large material removal rate (Shirk and Molian, 1998). These distinct features are attracting worldwide interest in the scientific research community and industry (Hopkins and Sibbett, 2000).

* Corresponding author. Tel.: +1-505-853-3184; fax: +1-505-846-1625.
E-mail address: jinn-kuen.chen@kirtland.af.mil (J.K. Chen).

0020-7683/02/$ - see front matter
PII: S0020-7683(02)00242-1

The phenomena of ultrashort laser interaction with solid matter are very different from those of conventional laser pulses longer than 100 ps (100×10^{-12} s). For the latter, thermal energy diffuses into deeper parts of a solid target, which reduces the energy density near the surface and broadens the energy distribution as well. Because plasma expansion and the later vaporization process create a strong recoil pressure that expels the melted material sideways, the material removed in the liquid phase creates drops on the target surface and a ''corona'' around the entrance hole (Momma et al., 1996). Basically, conventional laser-material removal is by thermal ablation wherein the material is locally heated to near boiling point. For the ultrashort laser interaction, it is observed that a thin layer of material is removed from the bulk with very little collateral damage (Momma et al., 1996; Perry et al., 1999). Plasma is produced, but hydrodynamic motion in the material is negligible. It is thus believed that the process of material removal is faster than that of heat conduction in the bulk material. Nonetheless, a complete understanding of the ultrafast laser-material ablation mechanisms is still missing.

Although numerous theories have been proposed to describe the ultrashort laser interaction with solid matter, most of them have been focused on thermal transport. Among which, the two-step heating models for metals (Kaganov et al., 1957; Anisimov et al., 1974; Qiu and Tien, 1992, 1993; Chen and Beraun, 2001), the thermal wave theories for semiconductors, dielectric crystals and insulators (Joseph and Preziosi, 1989, 1990; Tzou, 1992; Özisik and Tzou, 1994), and the dual-phase-lag model (Tzou, 1995a,b, 1997) for the above two categories of material are well established. Recently, two review articles by Hetnarski and Ignaczak (1999, 2000) have summarized five non-classical approaches that include the relaxation time effects in dynamic thermoelasticity. However, none of them is able to truly capture the important features of the ultrafast deformation and damage as mentioned previously.

For metal films heated by an ultrashort-pulsed laser, the hot-electron blast force, which is induced by hot-electron gas, could play an important role in the ultrafast deformation during picosecond transient. Falkovsky and Mishchenko (1999) find that the hot-electron blast force is proportional to the gradient of the electron-temperature squared. Due to the fact that the heat capacity of electrons is about two orders of magnitude smaller than that of a metal lattice, the excited electrons could shoot up to a very high temperature while the lattice primarily remains thermally undisturbed. Because the optical penetration (or skin) depth of metals is very small (in sub-microns), the gradient of the electron-temperature squared could be very sharp. This would result in a considerably large hot-electron blast force, and thereby causing severe lattice deformation. Therefore, we believe that the hot-electron blast force can be a vital power that destroys a thin layer of material near the irradiated surface before thermal energy conducts into the bulk as experimentally observed. The other important effect on the ultrafast deformation is the classical thermal load that results from non-uniform lattice temperature. In spite of the fact that the lattice temperature is fairly low in the early stage of ultrashort laser-material interactions, the lattice temperature gradient could be immense owing to the small size of thin films. Hence, the resulting thermal load could be substantial and would compound significantly the hot-electron blast effect on the thermomechanical behavior. This is particularly true for the late time response. Another interesting phenomenon is the strain rate effect. Because the ultrafast deformation occurs in such a short time period (sub-picoseconds to picoseconds), the strain rate could be extremely high. Consequently, the interconvertibility of the thermal and mechanical energy in metal lattices may not be neglected.

This work extends the dual-hyperbolic two temperature (Chen and Beraun, 2001) and hot-electron blast (Falkovsky and Mishchenko, 1999) models to study the ultrafast thermomechanical behaviors of a metal film subjected to femtosecond laser heating. The proposed, fully coupled thermomechanical model incorporates the hot-electron blast force and the classical thermal load into the momentum equations for the lattice deformation and the thermal–mechanical coupling into the lattice energy balance equation. To model ultrafast deformation in metal films heated locally by a uniform laser pulse, a set of one-dimensional (1D) transient thermoelasticity equations is derived based on the assumption of uniaxial strain but 3D stress. The time-dependent partial differential equations are solved with a central difference scheme to

evaluate the spatial derivatives and a forward difference scheme to estimate the time derivatives. Numerical analysis is performed with gold films ranging in thickness from 20 nm to 1.0 μm. The results, including the electron and lattice temperatures, hot-electron blast force, velocity, and stresses in the lattice, are presented. Two potential damage mechanisms, thermal (melting) and non-thermal (high stress), are discussed.

2. Hot-electron blast force

Recently, Falkovsky and Mishchenko (1999) have pioneered a hot-electron blast model for ultrafast deformation in metal films based on the Boltzmann equation and the Fermi–Dirac partition function. Because it is too difficult to solve the highly non-linear, coupled Boltzmann and thermoconductivity equations, they simplify the problem by assuming that there is no thermal coupling between electrons and the phonons. A dominating contribution to the hot-electron blast force that comes from the local equilibrium partition function is thus identified. Consequently the perturbation terms in the Boltzmann equation can be neglected. Several other simplifications are further made; however, the mathematics involved in the development of the hot-electron blast force is still quite complex. Therefore the hot-electron blast force is derived in an approximation form. For brevity, only the equations that are necessary in describing the hot-electron blast model are given below. Readers who are interested in the model development should refer to Falkovsky and Mishchenko (1999).

The linearly elastic equations of motion for ultrafast lattice deformation during the non-equilibrium stage proposed by Falkovsky and Mishchenko (1999) are given as

$$\rho \frac{\partial^2 u_i}{\partial t^2} = \lambda_{ijmn} \frac{\partial^2 u_m}{\partial x_j \partial x_n} + B_i, \quad i,j,m,n = 1,2,3 \tag{1}$$

where ρ is the mass density of a metal lattice, u_i are the displacement components, λ_{ijlm} are the elastic constants, x_i and t are the spatial coordinates and time respectively, and B_i are the hot-electron blast force components. A repeated spatial index refers to summation throughout this paper unless mentioned otherwise. In powers of (T_e/ε_F) up to the second order with T_e and ε_F respectively denoting the electron temperature and the Fermi energy, Falkovsky and Mishchenko (1999) showed that

$$B_i = \left[\frac{1}{32\pi} \frac{\partial}{\partial \varepsilon_F} \int \frac{\lambda_{ij}(\bar{p})}{v_F} \, dS_F \right] \left(\frac{\partial T_e^2}{\partial x_j} \right) \tag{2}$$

in which $\lambda_{ij}(\bar{p})$ represents the deformation potential with $\bar{p}$ denoting the electron momentum, v_F is the Fermi velocity, and S_F is the Fermi surface. Eq. (2) indicates that the hot-electron blast force is proportional to the gradient of electron-temperature squared.

The energy integral of the deformation potential over the Fermi surface given by Eq. (2) can be evaluated for various metals provided that all the physical properties involved are known. Hence, an explicit form for the hot-electron blast force can be derived. Whereas such an explicit expression is not available yet, the order of magnitude of B_i for noble metals has been estimated (Falkovsky and Mishchenko, 1999):

$$B_i = 2\Lambda_{ij} T_e \frac{\partial T_e}{\partial x_j}, \quad \Lambda_{ij} \sim g C_{eo} \delta_{ij} \tag{3}$$

In the above equation δ_{ij} is the Kronecker delta function, $g \sim 1$ is the dimensionless electron–phonon coupling constant, and C_{eo} is a constant characteristic in the temperature-dependent electron heat capacity C_e (Kittle, 1967),

$$C_e(T_e) = C_{eo} T_e \tag{4}$$

Because the thermal coupling between electrons and phonons as well as the thermal load resulting from lattice temperature are excluded, the above Falkovsky and Mishchenko's deformation model is only suitable for the very early time response of an ultrashort laser heating.

3. Two-step heat conduction

The hot-electron blast force, which dominates the non-equilibrium lattice expansion in the early time of an ultrashort laser-material interaction, depends upon not only the electron temperature but also the electron-temperature gradient (see Eq. (3)). In addition, the thermal load resulting from non-uniform lattice temperature could be another important source that compounds the lattice deformation at late times. Therefore, an accurate description of both the electron and lattice temperature fields is needed in order to precisely predict the ultrafast thermomechanical response.

When the transient time of thermal response from an ultrashort laser heating is comparable to or shorter than the characteristic time in electron-to-phonon collision (sub-picoseconds to few picoseconds for metals), the classical Fourier diffusion law would underestimate electron temperature but overestimate the lattice temperature before the thermal system reaches equilibrium (Chen and Beraun, 2001). To characterize the non-equilibrium behaviors of the electron and lattice temperatures in metals, Kaganov et al. (1957) first theoretically investigates the thermal coupling between electrons and phonons. Later, a phenomenological parabolic two-step heat conduction model is proposed by Anisimov et al. (1974). Because the heat conduction in metal lattices is not taken into account, the parabolic two-step model cannot accurately capture the lattice temperature response, especially for the late time. On a quantum mechanical and statistical basis, Qiu and Tien (1993) derive a more rigorous hyperbolic two-step radiation heating model, in which the micro-scale constitutive equations for electrons are in the same form as the Cattaneo–Vernotte thermal wave model (Tzou, 1997). Since Qiu and Tien's model (1993) accounts for the ballistic heat transport through electron gas, it describes better results than Anisimov et al. model (1974) for those laser pulse durations comparable to the electron relaxation time (sub-femtoseconds to tens femtoseconds for metals, depending on the electron and phonon temperatures). Chen and Beraun (2001) propose a dual-hyperbolic two-temperature model, which is an extension of the Qiu and Tien's theory (1993) by including the relaxation behavior of and the heat conduction in phonons. Basically the two-step heating models describe that the incident laser energy excites the electrons that are located within the skin depth. Then, a portion of the thermal electron energy transfers to the neighboring lattice, whereas another part of the energy diffuses, through electrons, into the deeper region of the material. Once the laser pulse passes away, the thermal coupling between the electrons and phonons as well as the heat conductions in the electrons and lattice continue until an equilibrium, steady state is established. For convenience, the acronym "DHTTM" is used for the dual-hyperbolic two-temperature model (Chen and Beraun, 2001) in the following sections.

In this work, the most general two-temperature theory DHTTM is extended to model the electron and lattice thermal transport (and the ultrafast lattice deformation) in a metal film under ultrashort laser heating. The following is a summary of the DHTTM in the 3D form:

$$C_{\mathrm{e}}(T_{\mathrm{e}})\frac{\partial T_{\mathrm{e}}}{\partial t} = -\nabla\cdot\bar{\boldsymbol{q}}_{\mathrm{e}} - G(T_{\mathrm{e}} - T_{\mathrm{l}}) + Q \tag{5}$$

$$\tau_{\mathrm{e}}\frac{\partial \bar{\boldsymbol{q}}_{\mathrm{e}}}{\partial t} + \bar{\boldsymbol{q}}_{\mathrm{e}} = -K_{\mathrm{e}}\nabla T_{\mathrm{e}} \tag{6}$$

$$C_{\mathrm{l}}(T_{\mathrm{l}})\frac{\partial T_{\mathrm{l}}}{\partial t} = -\nabla\cdot\bar{\boldsymbol{q}}_{\mathrm{l}} + G(T_{\mathrm{e}} - T_{\mathrm{l}}) \tag{7}$$

$$\tau_l \frac{\partial \bar{q}_l}{\partial t} + \bar{q}_l = -K_l \nabla T_l \tag{8}$$

where T denotes temperature, $\bar{q}$ is the heat flux vector, τ is the relaxation time, C is the heat capacity, K is the thermal conductivity, G is the electron–lattice coupling factor, Q is the volumetric laser heat source, and ∇ is the divergence operator. The quantities with subscripts e and l are associated with the electron and lattice, respectively.

The deposition of laser energy directly affects the electron-temperature field and in turn, the hot-electron blast force and the lattice temperature. Because ultrafast thermomechanical response strongly depends upon the hot-electron blast force and the lattice temperature distribution, the volumetric laser heat source should be characterized properly. In this work a flat-top laser beam (uniform intensity over the entire laser spot) is considered. Referring to the cylindrical coordinate, a mathematical form for the volumetric laser heat source resulting from a flat-top beam with a finite spot size is expressed as

$$Q(r,z,t) = \sqrt{\frac{\beta}{\pi}} \frac{(1-\delta)J_o}{t_p z_s} [u(r) - u(r-r_o)] \exp\left[-\left(\frac{z}{z_s}\right) - \beta\left(\frac{t-2t_p}{t_p}\right)^2 \right] \tag{9}$$

in which r and z are the radial and axial coordinates respectively, J_o is the peak fluence (at $r = z = 0$) carried by the laser pulse, δ is the surface reflectivity, t_p is the laser pulse duration defined as the full width of the laser pulse at the half maximum intensity, z_s is the optical penetration depth, $u(r)$ and $u(r-r_o)$ are Heaviside step functions, r_o is the spot radius, and $\beta = 4\ln(2)$.

As indicated in Eq. (9), the temporal profile of the laser pulses is assumed to be Gaussian. The laser beam is applied on the front surface ($z = 0$) at $t = 0$, and the peak laser intensity occurs when $t = 2t_p$. The intensities at $t = 1.5t_p$ and $2.5t_p$, $1.0t_p$ and $3.0t_p$, and 0.0 and $4.0t_p$ are 50%, 6.25% and ~0.0% of the peak value, respectively. The intensity of the volumetric laser heat source attenuates with an exponential function, $\exp(-z/z_s)$, as the depth increases.

4. Ultrafast thermoelasticity model

To investigate the ultrashort laser-induced thermomechanical response, a new ultrafast thermoelasticity model, abbreviated as UTEM, is formulated in this section. Let us consider a metal film irradiated locally by a flat-top laser beam on the front surface. The heated spot is finite, and the size is much larger than the film thickness. In view of the fact that ultrafast deformation takes place in a very short period of time, it is assumed that both the thermal transport and the lattice deformation do not occur immediately in directions normal to the thickness direction. Therefore, within the heated spot the thermal transport can be treated as a 1D process and the mechanical response is in a state of uni-axial strain but 3D stress. As similar to the shock waves induced by high velocity plate impact (Nicholos and Recht, 1990), the assumption of the 1D motion in the thickness direction within the heated region is appropriate until the lateral waves reflect back to the heated area. Since the lateral dimensions of a thin film are much larger than the film thickness, the time, which is of interest in this study, is much shorter than the time for the lateral waves to travel to the boundary and bounce back to interact with the 1D motion.

The state of uni-axial strain considered here is

$$\varepsilon_{zz}(z,t) \neq 0, \quad \varepsilon_{xx} = \varepsilon_{yy} = \varepsilon_{xy} = \varepsilon_{yz} = \varepsilon_{zx} = 0 \tag{10}$$

In this case the time rate of change of the lattice dilation $\dot{\varepsilon}_{kk}$ is the same as the strain rate $\dot{\varepsilon}_{zz}$.

The normal stress–normal strain relations for an isotropic material thus becomes

$$\sigma_{xx} = \sigma_{yy} = \lambda\varepsilon_{zz} - (3\lambda + 2\mu)\alpha(T_l - T_{lo}) \tag{11}$$

$$\sigma_{zz} = (\lambda + 2\mu)\varepsilon_{zz} - (3\lambda + 2\mu)\alpha(T_l - T_{lo}) \tag{12}$$

In the above two equations σ_{ii} ($i = x$, y, or z; no summation is applied) is the normal stress component in the i-direction, λ is the Lamé constant, μ is the shear modulus, α is the thermal expansion coefficient, and T_{lo} is a reference temperature for metal lattices. Since all shear stresses are null, the effective stress σ_e, which is a measurement for plastic deformation and may be used as an indicator for material failure, is simplified to

$$\sigma_e = |\sigma_{zz} - \sigma_{xx}| = 2\mu|\varepsilon_{zz}| \tag{13}$$

Eq. (13) shows that the effective stress is linearly proportional to the absolute value of the total strain ε_{zz}.

Since the non-equilibrium lattice deformation is induced in an extremely short period of time, one may anticipate that the time rate of change of the lattice dilation could be on the order of magnitude same as that of the lattice temperature. For that reason, the exchange of the thermal and mechanical energy in lattices should be accommodated. In addition, the classical thermal load that results from non-uniform lattice temperature may not be neglected due to the fact that lattice temperature gradient over a thin film could be considerably large even though the lattice temperature is small. To accurately describe the ultrafast thermomechanical response, therefore, we incorporate the classical thermal load into the hot-electron blast model (Eq. (1)) and the coupling between the volume change rate and the lattice temperature into the lattice energy balance Eq. (7) of the DHTTM. Since the electron and lattice temperatures as well as the lattice deformation are functions of z and t only, a set of fully coupled equations for ultrafast thermoelasticity under the uniaxial strain condition are then derived:

$$C_e(T_e)\frac{\partial T_e}{\partial t} = -\frac{\partial q_e}{\partial z} - G(T_e - T_l) + Q(z,t) \tag{14}$$

$$\tau_e\frac{\partial q_e}{\partial t} + q_e = -K_e\frac{\partial T_e}{\partial z} \tag{15}$$

$$C_l(T_l)\frac{\partial T_l}{\partial t} = -\frac{\partial q_l}{\partial z} + G(T_e - T_l) - (3\lambda + 2\mu)\alpha T_l\dot{\varepsilon}_{kk} \tag{16}$$

$$\tau_l\frac{\partial q_l}{\partial t} + q_l = -K_l\frac{\partial T_l}{\partial z} \tag{17}$$

$$\rho\frac{\partial^2 u_z}{\partial t^2} = (\lambda + 2\mu)\frac{\partial^2 u_z}{\partial z^2} - (3\lambda + 2\mu)\alpha\frac{\partial T_l}{\partial z} + 2\Lambda_{zz}\left(T_e\frac{\partial T_e}{\partial z}\right) \tag{18}$$

In Eqs. (14)–(18) q_e and q_l are the heat fluxes in the z-direction respectively, and u_z is the lattice displacement. Note the differences between Eqs. (16) and (7) and between (18) and (1). In general, the present UTEM is suitable for describing the entire time histories of electron and lattice temperatures as well as mechanical responses for an ultrashort (and also longer) pulsed laser heating on metal materials.

The governing Eqs. (14)–(18) will be solved under proper initial and boundary conditions. For simplicity, the problem considered here is a metal film that is initially at rest and at a uniform temperature. Thus, one has the following initial conditions,

$$u_z(z,0) = 0, \quad \frac{\partial u_z(z,0)}{\partial t} = 0, \quad \text{and} \quad \sigma_{xx}(z,0) = \sigma_{yy}(z,0) = \sigma_{zz}(z,0) = 0 \tag{19}$$

$$T_e(z,0) = T_l(z,0) = T_{lo} \tag{20}$$

In this study T_{lo} is set at room temperature (300 K).

During the ultrashort laser heating process, heat losses to the front and back surfaces are assumed to be negligible (Qiu and Tien, 1992, 1993), implying that

$$q_e(0,t) = q_e(L,t) = 0 \tag{21}$$

where L is the film thickness. For the mechanical response, it is assumed that the front and back surfaces of the film are stress free. Thus,

$$\sigma_{zz}(0,t) = \sigma_{zz}(L,t) = 0 \tag{22}$$

5. Thermophysical properties

In the present study, the fast-transient temperatures ranging from room temperature to the Fermi temperature (the order of 10^4 K for metals) for electrons and to the melting point for the lattice are of interest. Thermal properties of energy carriers, including both electrons and the lattice in the metal material, will sensitively vary with temperature over a wide range in the picosecond domain. However, for simplicity, the mechanical properties of the metal lattice, including the elastic moduli, density and thermal expansion coefficient, will be assumed to be constant because their variations with respect to temperature in the condition of extremely high strain rate remain unknown.

For electrons, three thermophysical properties are temperature quite sensitive: the heat capacity, relaxation time and thermal conductivity. Eq. (4) shows the electron heat capacity as a linear function of electron temperature. The following is a general form for the electron thermal conductivity (Kittle, 1967)

$$K_e = \frac{\pi^2 n_e k_B^2 T_e \tau_e}{3 m_e} \tag{23}$$

where n_e is the number density of electrons per unit volume, m_e is the mass of an electron, and k_B is the Boltzmann's constant. Eq. (23) shows that the electron thermal conductivity is linearly proportional to the electron temperature and the relaxation time. For good conductors, the electron–electron scattering rate $\tau_{e\text{-}e}(= A_e T_e^2)$ and the electron–phonon scattering rate $\tau_{e\text{-}l}(= B_l T_l)$, where A_e and B_l are constant, both contribute to the electron collision frequency. A relationship between the electron relaxation time τ_e and the electron–electron and electron–phonon scattering rates for electron temperatures that do not exceed the Fermi temperature is given by (Wang et al., 1994)

$$\tau_e = \frac{1}{A_e T_e^2 + B_l T_l} \tag{24}$$

For the electron temperature being higher than the Fermi temperature, the dependence of electron temperature on τ_e is $T_e^{-3/2}$ (Anismov and Rethfeld, 1997). For gold, the Fermi temperature is 6.42×10^4 K and the two constants for the scattering rates are: $A_e = 1.2 \times 10^7$ $\mathrm{K^{-2}\,s^{-1}}$ and $B_l = 1.23 \times 10^{11}$ $\mathrm{K^{-1}\,s^{-1}}$ (Wang et al., 1994). By substituting the values of A_e and B_l into Eq. (24), the calculated electron relaxation time of gold is about 27.0 fs (27.0×10^{-15} s) for electrons at room temperature and about 0.02 fs at the Fermi temperature.

Neglecting the term $A_e T_e^2$ in Eq. (24) and substituting the result into (23) yields

$$K_e = K_{eo}\left(\frac{T_e}{T_l}\right) \tag{25}$$

The above equation has been widely used in the two-step heat conduction modeling. It should be noted that this linear relationship is only adequate for low electron temperature.

Because the electron density n_e depends upon the electron temperature and needs to be determined, Eq. (23) is not in a form yet that can be directly applied in the present numerical analysis. Therefore,

another relationship for K_e that covers over a wide range of electron temperature (Anismov and Rethfeld, 1997) is considered here

$$K_e = \chi \frac{(\vartheta_e^2 + 0.16)^{5/4}(\vartheta_e^2 + 0.44)\vartheta_e}{(\vartheta_e^2 + 0.092)^{1/2}(\vartheta_e^2 + \eta\vartheta_l)} \tag{26}$$

where $\vartheta_e \equiv T_e/T_F$ and $\vartheta_l \equiv T_l/T_F$ are the normalized electron and lattice temperatures with T_F denoting the Fermi temperature; χ and η are material constants. Two extreme cases can be derived (Anismov and Rethfeld, 1997). For high electron temperatures $\vartheta_e \gg 1$, Eq. (26) results in the well-known dependence $K_e \sim T_e^{5/2}$, which is characteristic for low-density plasma. In the low electron-temperature limit $\vartheta_e \ll 1$, Eq. (26) reduces to the linear Eq. (25).

The temperature-dependent thermal conductivity and heat capacity of a gold lattice over the range from room temperature to the melting point are listed in Table 1. The values in the parenthesis are the bulk heat capacity C (Touloukian et al., 1970; Touloukian and Buyco, 1970) and C_l is calculated using the relationship $C = C_e + C_l$. A linear distribution is assumed for the properties between any two consecutive data in Table 1. The other thermophysical properties involved in the UTEM, volumetric laser heat source Eq. (9), electron heat capacity Eq. (4), and electron thermal conductivity Eq. (26) are as follows (Qiu and Tien, 1993; Anismov and Rethfeld, 1997; Tzou, 1997): $C_{eo} = 70\ \mathrm{J\,m^{-3}\,K^{-2}}$, $G = 2.6 \times 10^{16}\ \mathrm{W\,m^{-3}\,K^{-1}}$, $\tau_l = 38.7$ ps, $\delta = 0.93$, $z_s = 15.3$ nm, $\chi = 353\ \mathrm{W\,m^{-1}\,K^{-1}}$, and $\eta = 0.16$. Since $\Lambda_{zz} \sim gC_{eo}$ with g being of the order of unity, referring to Eq. (3), $\Lambda_{zz} \sim gC_{e0} = 70\ \mathrm{J\,m^{-3}\,K^{-2}}$. The phonon relaxation time of 38.7 ps is computed by using Eq. (1.37) in Tzou (1997). The reflectivity of 0.93 and the optical penetration depth of 15.3 nm are the typical values for visible light. It is also noted that Eq. (26) gives K_e a value of $315\ \mathrm{W\,m^{-1}\,K^{-1}}$ at room temperature, which is identical to the bulk material conductivity. The gold's melting temperature is 1337 K.

In passing, note that Eqs. (14) and (15) (for electrons), Eqs. (16) and (17) (for phonons), and Eq. (18) (for acoustic displacement) involve three interweaving waves. Due to the significantly different relaxation times by orders of magnitude between τ_e (on the order of femtoseconds) and τ_l (on the order of picoseconds), the thermal wave behavior in electrons (in femtoseconds) already diminishes as the thermal and mechanical interactions take place in the picosecond domain. The wave interactions in the picosecond domain, therefore, are only described by Eqs. (16)–(18), which has been studied in detail in the wave theory of heat conduction (Achenbach, 1968; Tzou, 1995b).

Existence and uniqueness of the solutions to Eqs. (14)–(22) with constant thermomechanical properties (Tzou, 1997) as well as the domains of influence in correspondence have been proven in the development of the dual-phase-lag model. Dominating groups are identified in terms of two characteristic times describing the delayed response, which, numerically, allow changes of the involved thermomechanical properties over a wide range. In presence of the temperature-dependent thermal properties as shown in Eqs. (14)–(17), these

Table 1
Conductivity and heat capacity of gold lattice

T (K)	k_l (W/mK)[a]	C_l ($10^6\ \mathrm{J\,m^{-3}\,K^{-1}}$)
300	315	2.479 (2.50)
604		2.708 (2.75)
636	271	
964	246	
1017		2.839 (2.91)
1100	234	
1337	176	
1373		2.726 (2.82)

Values in the parentheses are the bulk property (Touloukian and Buyco, 1970).
[a] Touloukian et al. (1970).

properties do vary but their instantaneous values lie within the admissible range as long as their values do not reduce to zero. Note that the value of T_e ultimately reduces to that of T_l at thermal equilibrium. The energy exchange terms (led by G) in Eqs. (14) and (16) vanish in this case and all thermal properties recover their non-zero equilibrium values. A bifurcated solution will not exist because the diminution of the energy exchange, both are low-order terms in Eqs. (14) and (16), does not alter the characteristics of the equations.

6. Numerical results and discussion

Due to the strong non-linearity of the coupled transient equations and the temperature-dependent thermophysical properties, it is impossible to derive closed-form solutions to the present UTEM. Therefore, the governing Eqs. (14)–(18), together with the volumetric heat source, Eq. (9) with $r_o \to \infty$, and the initial and boundary conditions, Eqs. (19)–(22), are solved by using a central difference scheme to evaluate the spatial derivatives and a forward difference scheme to estimate the time derivatives. Discussion on the accuracy and stability of these schemes can be found in textbooks (Anderson et al., 1984, for example).

For wave propagation problems that are solved with a finite difference method, the numerical solutions often exhibit spurious (V-shape) oscillation (Anderson et al., 1984; Meyers, 1994). To remove the oscillation, an artificial viscosity is introduced in this work

$$\Pi = \omega_l \rho V_s \Delta z \left| \frac{\partial \dot{u}_z}{\partial z} \right| - \rho(\omega_Q \Delta z)^2 \left| \frac{\partial \dot{u}_z}{\partial z} \right| \frac{\partial \dot{u}_z}{\partial z} \tag{27}$$

where $\dot{u}_z$ is the velocity of a metal lattice, V_s is the speed of sound, and the two constants $\omega_l = 0.1$–0.3 and $\omega_Q = 2.0$ (Meyers, 1994). Thus, the momentum Eq. (18) is modified to

$$\rho \frac{\partial^2 u_z}{\partial t^2} = (\lambda + 2\mu) \frac{\partial^2 u_z}{\partial z^2} - (3\lambda + 2\mu)\alpha \frac{\partial T_l}{\partial z} + 2\Lambda_{zz} \left(T_e \frac{\partial T_e}{\partial z} \right) + \frac{\partial \Pi}{\partial z} \tag{28}$$

Local oscillations in the electron and lattice temperatures are minor. For simplicity, they are smoothed out algebraically if occur.

Five gold films of 20, 50, 100, 200, and 1000 nm in thickness heated by laser beams having the same pulse width $t_p = 100$ fs are investigated. Uniform grids are employed. The corresponding numbers of the grid points meshed are 51, 51, 101, 201, and 501, and the time increments used are 0.025, 0.05, 0.1, 0.2, and 0.2 fs, respectively. The mechanical properties are: $\rho = 1.93 \times 10^4$ kg/m^3, $E = 74.9$ GPa, $v = 0.42$, and $\alpha = 14.2 \times 10^{-6}$ m/m (Trent et al., 1972). The value of ω_l is set to be 0.1 for the first two films and 0.3 for the rest. Numerical results, including the electron and lattice temperatures, hot-electron blast force, velocity, and thermal stresses, are presented and discussed in the following.

Fig. 1 shows the time histories of the electron and lattice temperatures at the front surface of a 1.0 μm gold film subjected to the laser heating at $J_o = 7147$ J/m^2. Two solutions, obtained from the thermal model DHTTM and the present thermomechanical model UTEM, are shown in the figure although they seem indistinguishable. The fluence J_o applied here is the melting threshold predicted from the DHTTM. At this level of J_o, the maximum lattice temperature obtained from the DHTTM occurs at the front surface and is equal to the melting point. Because it just starts to melt, the value of the fluence is referred as the melting threshold (Wellershoff et al., 1999). It is clearly seen from Fig. 1 that the early stage of ultrafast laser heating is a non-equilibrium process, i.e., a state that the electron and lattice temperatures diverge significantly. The maximum electron temperatures calculated from the two models are almost identical, 2.681×10^4 K, and occurs at almost the same time, $t = 0.284$ ps (shortly after the laser pulse passes its peak irradiance, at $t = 0.2$ ps). At this time instant, the computed lattice temperatures are already slightly different, 332.0 K by the DHTTM versus 331.1 K by the UTEM. Owing to the high strain-rate effect, a significant difference of

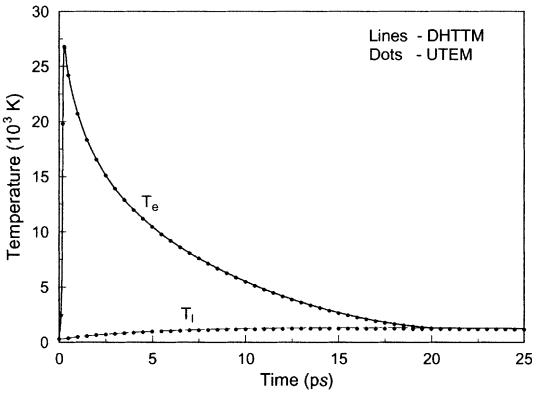

Fig. 1. Time histories of the electron and lattice temperatures at the front surface of a 1.0 μm gold film heated by a laser pulse with $t_p = 100$ fs and $J_o = 7147$ J/m^2.

the maximum lattice temperature between the two models is anticipated. They are found to be 1337 K occurring at about $t = 15.80$ ps for the DHTTM and 1249 K occurring at about $t = 15.18$ ps for the UTEM. Further UTEM analysis yields another value of 7790 J/m^2 for the melting threshold, about 9.0 % higher than that obtained from the DHTTM.

The results in Figs. 2–10 are calculated for the 1.0 μm film heated by the laser pulse at the melting threshold $J_o = 7790$ J/m^2. Fig. 2 depicts the electron-temperature distribution over the first half of the domain ($z = 0$–500 nm). It appears that both the electron temperature and the electron-temperature gradient increase rapidly before the temperature reaches the maximum value, 2.809×10^4 K, at approximately $t = 0.284$ ps and then decrease at a slower rate as time prolongs. The lattice temperature distribution is plotted in Fig. 3. Contrast to the electron temperature, the lattice temperature rises much slower due to the fact that the heat capacity of the gold lattice is about two orders of magnitude larger than that of the electrons. The lattice temperature reaches the melting point at a later time, around $t = 15.91$ ps.

The hot-electron blast force is presented in Fig. 4. Apparently, the hot-electron blast force develops rapidly in a small region near the irradiated surface and quickly reaches the maximum value, -2.281×10^{18} N/m^3, at about $t = 0.271$ ps (slightly earlier than the time when the maximum electron temperature occurs,

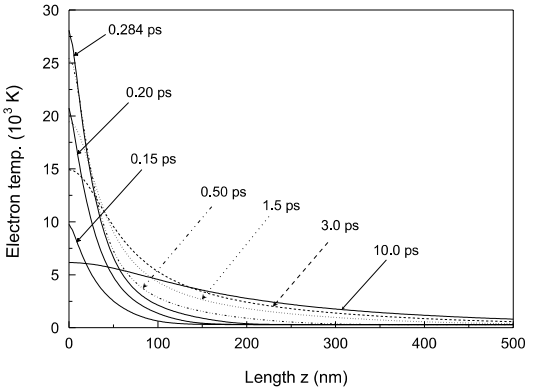

Fig. 2. Electron-temperature distribution in the first half of a 1.0 μm gold film heated by a laser pulse with $t_p = 100$ fs and $J_o = 7790$ J/m^2.

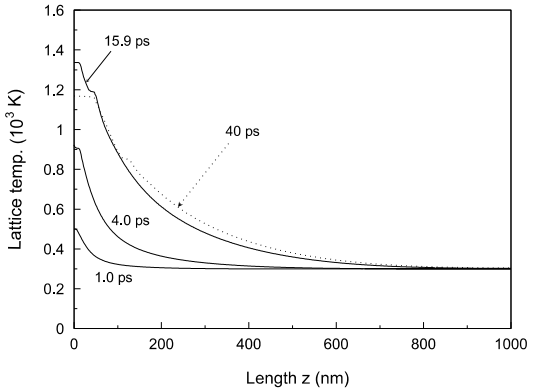

Fig. 3. Lattice temperature distribution in a 1.0 μm gold film heated by a laser pulse with $t_p = 100$ fs and $J_o = 7790$ J/m^2.

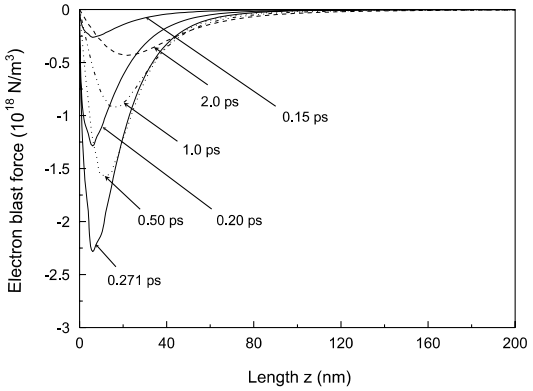

Fig. 4. Hot-electron blast force in the first fifth of a 1.0 μm gold film heated by a laser pulse with $t_p = 100$ fs and $J_o = 7790$ J/m^2.

see Fig. 2). During this extremely short period of time, the peaks of the force occur at the same location $z = 6.0$ nm, recalling that the optical penetration depth is 13.5 nm. As time increases, the force decreases swiftly and the peak shifts deeper inside the film. When $t = 2.0$ ps, for instance, the peak moves to the location $z = 22.0$ nm and the magnitude reduces to -0.430×10^{18} N/m^3. Development and transient of the hot-electron blast force can be elucidated by the electron-temperature distribution. According to Eq. (3), the blast force is proportional to the product of the temperature and the temperature gradient in the electron gas. As a result of the zero slope of the electron temperature at $z = 0$ and L (the boundary conditions of no heat loss), the force should vanish at both boundaries in spite of the fact that the maximum electron temperature occurs at the front surface. Hence, the peak of the hot-electron blast force must appear somewhere inside the film as shown in Fig. 4. The hasty rising and diminishing of the hot-electron blast force is in good correspondence with the swift response of the electron temperature.

Figs. 5 and 6 illustrate the thermal stress σ_{zz} computed with and without the hot-electron blast effect respectively. For clarity, only the results in the first fifth of the film ($z = 0$–200 nm) are presented here. Emphasis is placed on the response in the region of 0–50 nm. The difference of the stress responses in this localized area reveals the pronounced impact of the hot-electron blast force on the ultrafast deformation. It is also noted that the artificial viscosity suppresses the spurious oscillation in the stress (dashed lines with dots), which is calculated without the artificial viscosity. Fig. 7 shows the stress component $\sigma_{xx}(= \sigma_{yy})$ for

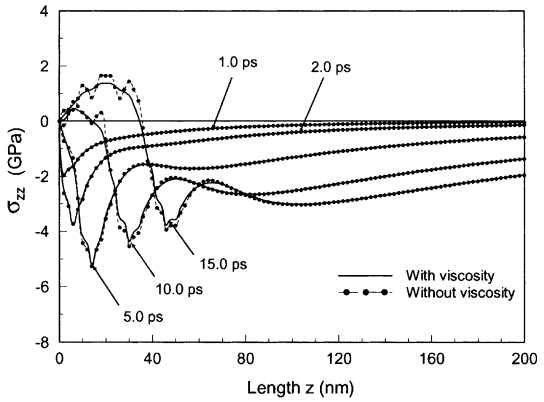

Fig. 5. Stress σ_{zz} in the first fifth of a 1.0 μm gold film heated by a laser pulse with $t_p = 100$ fs and $J_o = 7790$ J/m^2.

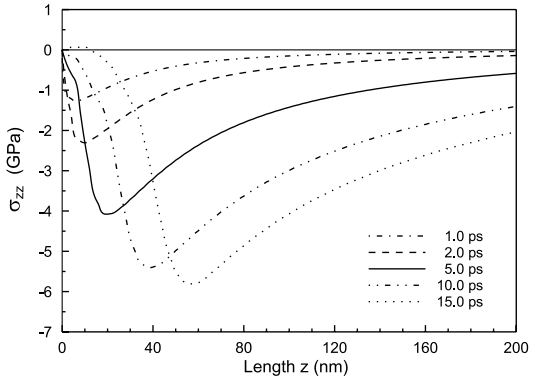

Fig. 6. Stress σ_{zz} in the first fifth of a 1.0 μm gold film heated by a laser pulse with $t_p = 100$ fs and $J_o = 7790$ J/m^2, calculated without the electron blast effect.

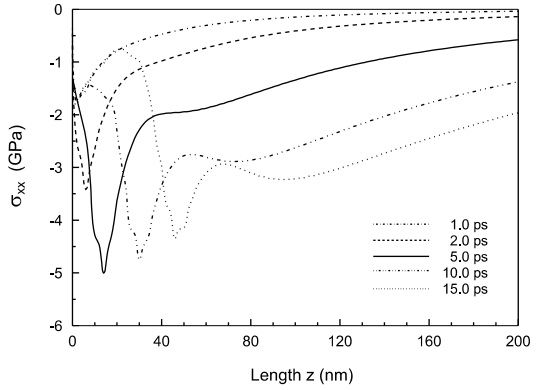

Fig. 7. Stress σ_{xx} in the first fifth of a 1.0 μm gold film heated by a laser pulse with $t_p = 100$ fs and $J_o = 7790$ J/m^2.

the case with the hot-electron blast effect. Interestingly, the distribution of σ_{xx} is similar to that of σ_{zz} except that σ_{zz} is zero at $z = 0$ in Fig. 5. With the stress free boundary condition for σ_{zz}, Eq. (12) gives the total strain ε_{zz} at $z = 0$ and L as

$$\varepsilon_{zz} = \frac{(3\lambda + 2\mu)\alpha(T_l - T_{lo})}{\lambda + 2\mu} \tag{29}$$

Substitution of Eq. (29) into (11) results in

$$\sigma_{xx} = \sigma_{yy} = -\frac{2\mu(3\lambda + 2\mu)\alpha(T_l - T_{lo})}{\lambda + 2\mu} \tag{30}$$

The above equation indicates that the two stress components σ_{xx} and σ_{yy} at the boundary are only functions of the lattice temperature. Since $T_l \succ T_{lo}$ for $t \succ 0$ considered in this study, both σ_{xx} and σ_{yy} are always compressive. At $t = 5.0$ ps, for example, the calculated lattice temperature at $z = 0$ is 1013 K and the stress $\sigma_{xx}(= \sigma_{yy})$ is 1.30 GPa, which is in excellent agreement with the value computed by directly substituting the lattice temperature into Eq. (30). A similar comparison of σ_{xx} (and σ_{yy}) with σ_{zz} is also found for the case without the hot-electron blast effect.

Due to the 3D stress nature, the effective stress σ_e may be a useful parameter for the material damage assessment. It is thus computed and shown in Fig. 8 for several time instants. Again, only the results over a portion of the domain $z = 0$–100 nm are demonstrated here for clarity. It is evident, due to the significant difference between the stress magnitudes found in Figs. 5 and 8, that use of the effective stress σ_e or a single stress σ_{zz} for the failure prediction would result in a very different conclusion of the damage. Fig. 9 represents the effective stress computed without the hot-electron blast force. It is interesting to compare the results in Figs. 8 and 9. The two effective stresses at the front surface are close but not identical. For instance, the values at $t = 10$ ps are 1.755 and 1.781 GPa for the cases with and without the hot-electron blast force, respectively. The difference could be attributed to the different lattice temperatures due to the different strain rates. This conjecture is verified by Eq. (30) with the corresponding lattice temperatures, 1263 and 1278 K.

As the effective stress is an indicator for damage, the velocity v_z in Fig. 10 provides useful information for whether the damaged material would be removed from or stay with the bulk material. The negative value of the velocity means that material moves along the $-z$-direction. Assume that the failure strength of gold is temperature- and rate-independent and equals that at room temperature, 1.24 GPa (Trent et al., 1972). By comparing the effective stress in Figs. 8 and 9 with the failure strength respectively, a first-order approximation of the damage length, for $t = 10$ ps for example, is about 21 nm for the case with the hot-electron

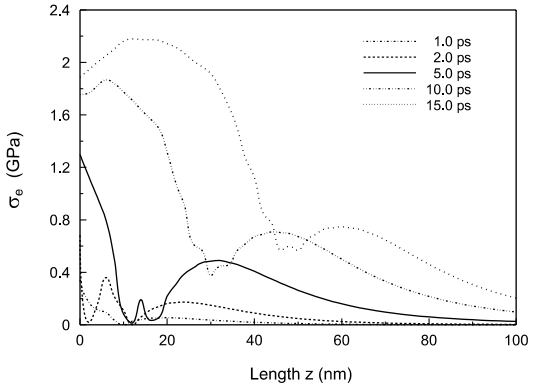

Fig. 8. Effective stress σ_e in the first tenth of a 1.0 μm gold film heated by a laser pulse with $t_p = 100$ fs and $J_o = 7790$ J/m^2.

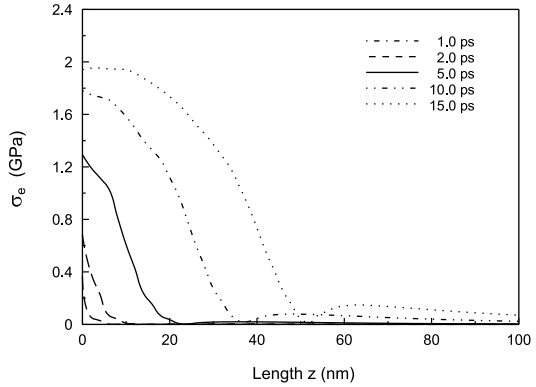

Fig. 9. Effective stress σ_e in the first tenth of a 1.0 μm gold film heated by a laser pulse with $t_p = 100$ fs and $J_o = 7790$ J/m^2, calculated without the electron blast effect.

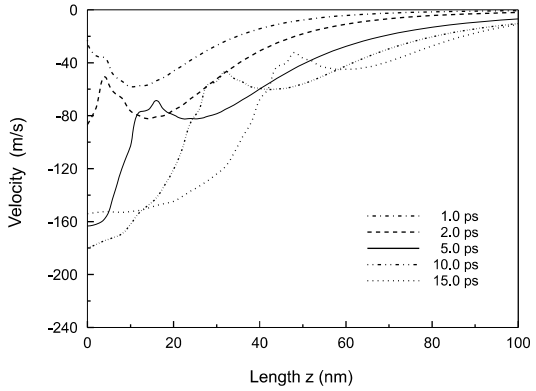

Fig. 10. Velocity v_z in the first tenth of a 1.0 μm gold film heated by a laser pulse with $t_p = 100$ fs and $J_o = 7790$ J/m^2.

blast effect and about 18 nm for the case without the blast effect. As suggested by the negative velocity in Fig. 10, any damaged material would be removed immediately from the bulk by that speed. Recalls that the predicted time for the onset of thermal melting at the front surface is about 15.91 ps. These results imply that non-thermal damage could occur before the material melts.

In reality, the ultrashort laser ablation is a continuous process even though it takes place in such a short period of time. Once a piece of material is damaged and removed, the thermal energy associated with the removed material, which must be a fairly large portion of the total energy that is absorbed by the film, is also removed. As a result, there might not be enough energy left to raise the lattice temperature to the melting point. In other words, thermal melting could never happen. If this is true, non-thermal damage from high stress would be the material ablation mechanism for a 1.0 μm film heated by a 100 fs laser pulse at the melting threshold fluence. Thus, the above argument can explain the experimental observation: (a) a thin layer of material is removed from the bulk material with minimal collateral thermal damage and (b) hydrodynamic motion is negligible (Momma et al., 1996; Perry et al., 1999).

Since the hot-electron blast force increases with laser fluence, a value of $J_o = 38,949$ J/m^2, five times the melting threshold, is investigated. At this fluence level, the theoretical maximum electron temperature increases to 6.424×10^4 K (close to the Fermi temperature 6.42×10^4 K), and the maximum hot-electron

blast force becomes -12.39×10^{18} N/m^3. For the lattice, the onset of thermal melting is at approximately $t = 2.44$ ps. Comparison of the data with those in the previous case of $J_o = 7790$ J/m^2 shows that a five-time fluence boosts the electron temperature by 2.29 times and the hot-electron blast force by 5.43 times but shortens the onset time of thermal melting by 6.52 times. The effective stress distributions resulting from this higher fluence are displayed in Figs. 11 and 12 for the time instants $t = 0.5$, 1.0, 1.5, 2.0, and 2.5 ps. Again, one of our interests is to examine the hot-electron blast effect. Fig. 12 shows that the computed effective stress is localized in the region very near the irradiated surface when the hot-electron blast force is neglected. This is because the interaction time is so short that heat scarcely conducts into the deeper part of the lattice. Like the lower fluence case, Fig. 12 gives the first-order approximation of the damage length only one (1) nm at $t = 2.0$ ps, for example. For the case with the hot-electron blast effect, on the other hand, there are two areas in which damage could occur. One is in the region of $z = 0$–10 nm, and the other is in the region around $z = 30$ nm. The first-order approximation of the damage length at $t = 2.0$ ps is about 9 nm for this case. It is also seen in Fig. 11 that at $t = 2.5$ ps, the peak stress in the region around 30 nm exceeds the strength 1.24 GPa. Because material is hardly removed if the hot-electron blast effect is excluded, thermal melting at the later time would be the dominating damage mechanism. Should this be the case, hydrodynamic motion will occur. This, then, contradicts to the experimental observations

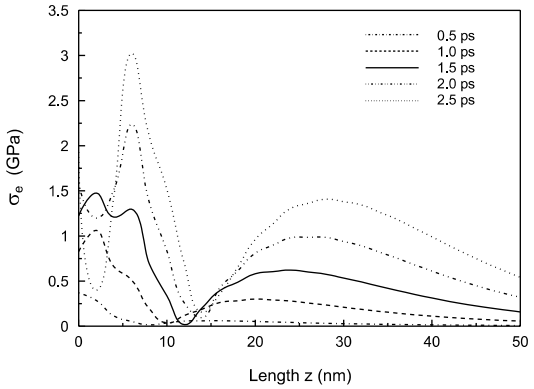

Fig. 11. Effective stress σ_e in the first twentieth of a 1.0 μm gold film heated by a laser pulse with $t_p = 100$ fs and $J_o = 38{,}949$ J/m^2.

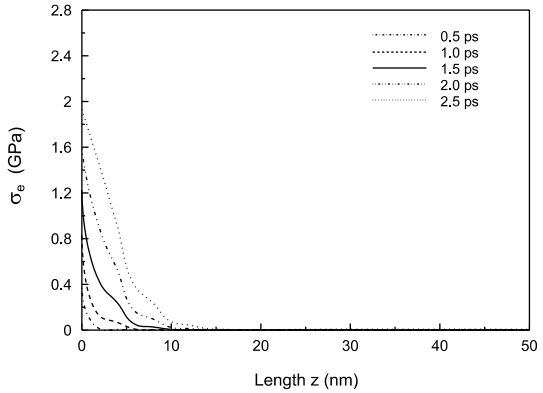

Fig. 12. Effective stress σ_e in the first twentieth of a 1.0 μm gold film heated by a laser pulse with $t_p = 100$ fs and $J_o = 38{,}949$ J/m^2, calculated without the electron blast effect.

(Momma et al., 1996; Perry et al., 1999). A similar conclusion to the 1.0 μm film case is found for a thinner, 200 nm gold film. For brevity, those results are not presented here.

Fig. 13 plots the effective stress as a function of z for a 100 nm film irradiated by the laser pulse at the melting threshold $J_o = 4442$ J/m^2. The onset of thermal melting in this case occurs at approximately $t = 29.3$ ps. As expected, the thermal model DHTTM predicts a lower melting threshold, 4133 J/m^2. It is worth noting that the magnitude of the effective stress in the rear region of the 100 nm film is quite different from those found in the thicker films. Clearly, the magnitudes of the effective stress in the two regions near the front and rear surfaces are comparable. This implies that non-thermal damage from the back surface is also possible if the laser is intense enough.

Further numerical analysis shows that the hot-electron blast effect on the ultrafast deformation is less pronounced for a 50 nm gold film than for the thicker films. This is evidenced in Fig. 14 by the slight difference between the two effective stresses computed with (solid lines) and without (dashed lines) the hot-electron blast force. The fluence used in the two calculations is 2215 J/m^2, which is the melting threshold obtained from UTEM. The onset of thermal melting is found at about $t = 45.3$ ps for this thinner film. It is clearly shown in Fig. 14 that the peak stress at the two boundaries occurring at $t = 5$ and 10 ps are below the strength (12.4 GPa). As time increases, the stress peak rapidly shifts to the middle region and reaches the maximum at approximately $t = 23$ ps. From $t = 13$ to 23 ps, the effective stress in the entire film exceeds

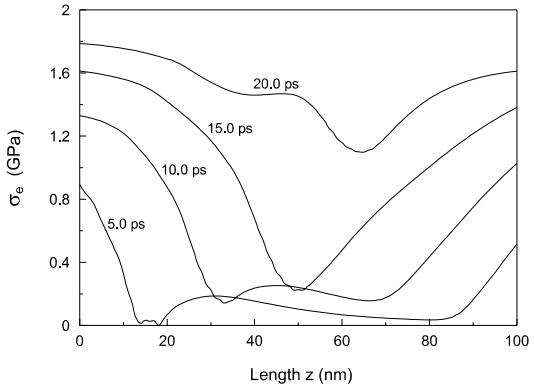

Fig. 13. Effective stress σ_e as a function of z for a 100 nm gold film heated by a laser pulse with $t_p = 100$ fs and $J_o = 4442$ J/m^2.

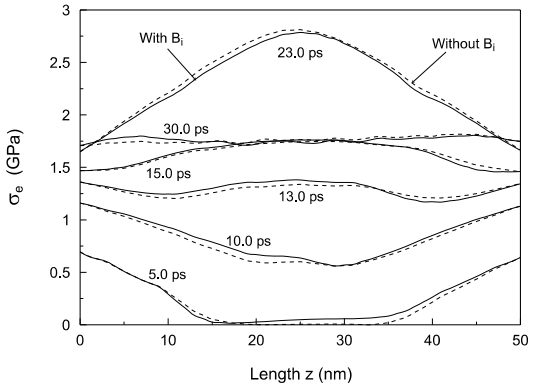

Fig. 14. Effective stress σ_e as a function of z for a 50 nm gold film heated by a laser pulse with $t_p = 100$ fs and $J_o = 2215$ J/m^2.

the failure strength. It is thus likely that for a 50 nm film heated by a 100 fs laser at the melting threshold fluence, non-thermal damage could initiate from the middle region and then extend to the whole film. However, it is also possible that damage first occurs in the regions near both the front and back surfaces if the laser intensity is intense enough, for instance, five times of the melting threshold. Similar damage situations are found for a further thinner, 20 nm film except that the peak stress occurs in the middle region earlier. Over again, those results are not presented for brevity.

It should be pointed out here that the physics involved in the ultrashort laser-material ablation process are complex and are not fully understood yet. The present work is a first attempt to identify the material damage mechanisms in this very complicated problem based on the dynamic thermomechanics. As we have found from this study, the strain rate is extremely high, on the order of 10^9 s^{-1}. Under such a high strain rate, it is very likely that metal materials would lessen its ductility and become more brittle. Furthermore, the embrittlement could alter the elastic limit. This is an interesting research subject though it has not been explored yet. The reason for assuming linear elasticity in this paper is primarily because of the lack of material data for such a harsh environment and also for mathematical simplicity. It should be reminded that the material damage and removal mechanisms addressed in this study are qualitative and need a further justification. As manufacturing technology progresses into the nano-scale era, interests and investigations in this area are expected in the future.

7. Conclusions

Ultrafast deformation in metal films heated by an ultrashort laser pulse is a highly non-equilibrium behavior. Unlike conventional dynamic thermoelasticity, the hot-electron blast force, which is generated by hot-electron gas, could play a crucial role in the lattice deformation. The other important factor is the thermal load that results from the temperature gradient in a metal lattice. Since the strain rate is extremely high, on the magnitude of 10^9 s^{-1}, the coupling between the thermal and mechanical energy in the lattice is also of very importance.

To investigate the thermomechanical response of metal films subjected to ultrashort-pulsed laser heating, this work incorporates the thermal load into the hot-electron blast model (Falkovsky and Mishchenko, 1999) and the coupling between the thermal and mechanical energy into the DHTTM (Chen and Beraun, 2001). A set of fully coupled, transient thermoelasticity equations is derived based on the condition of uniaxial strain but with 3D stress. The governing equations, together with the volumetric laser heat source and the initial and boundary conditions, are solved with a central difference scheme to estimate the spatial derivatives and a forward difference scheme to estimate the temporal derivatives. To suppress the spurious oscillation in thermal stresses caused from the finite difference method, an artificial viscosity is introduced.

Numerical analysis is performed with five gold films ranging in thickness from 20 nm to 1.0 μm. The laser pulse length is assumed to be $t_p = 100$ fs; the fluences that are equal to or beyond the melting threshold are considered. No mechanical constraint is imposed to the films. The numerical results show that the maximum hot-electron blast force is induced shortly after the laser pulse passes the peak irradiance. The impact of the hot-electron blast effect on the ultrafast lattice deformation is more pronounced for thicker films than for thinner films. Two potential material damage mechanisms, thermal (melting) and non-thermal (high-stress), are identified based on the effective stress criterion. For gold films thicker than 200 nm, non-thermal damage in a small region near the irradiated surface could be the dominating ablation mechanism. Neglecting the hot-electron blast effect could underestimate the potential of the non-thermal damage, especially for intensive laser pulses. For thinner films of 50 nm in thickness and less, an entire film could be destroyed before thermal melting takes place. Location of the damage initiation, either in the middle region or from the boundary, depends upon the laser intensity. In between the two categories, a 100 nm film for example, non-thermal damage could occur in the regions near the front and back surfaces.

This study provides an explanation about how the material in a gold film is damaged and removed by ultrashort laser pulses based on the thermomechanics approach. Because no stress–strain data is available for the material at extremely high strain rates, the damage assessed here is qualitative and subject to further justification. As manufacturing technology progresses into the nano-scale era, characterization of the temperature- and rate-dependent stress–strain behaviors at the strain rate of order 10^9 s^{-1} is needed.

References

Achenbach, J.D., 1968. The influence of heat conduction on propagation of stress jumps. J. Mech. Phys. Solids 16, 273–282.

Anderson, D.A., Tannehill, J.C., Pletcher, R.H., 1984. Computational Fluid Mechanics and Heat Transfer. McGraw-Hill, New York.

Anisimov, S.I., Kapeliovich, B.L., Perelman, T.L., 1974. Electron emission from metal surfaces exposed to ultra-short laser pulses. Sov. Phys. JETP 39, 375–377.

Anismov, S.I., Rethfeld, B., 1997. On the theory of ultrashort laser pulse interaction with metal. SPIE 3093, 192–203.

Chen, J.K., Beraun, J.E., 2001. Numerical study of ultrashort laser pulse interactions with metal films. Numer. Heat Transfer Part A 40, 1–20.

Falkovsky, L.A., Mishchenko, E.G., 1999. Electron-lattice kinetics of metals heated by ultrashort laser pulses. J. Exp. Theor. Phys. 88, 84–88.

Hetnarski, R.B., Ignaczak, J., 1999. Generalized thermoelasticity. J. Thermal Stress 22, 451–476.

Hetnarski, R.B., Ignaczak, J., 2000. Nonclassical dynamical thermoelasticity. Int. J. Solids Struct. 37, 215–224.

Hopkins, J.M., Sibbett, W., 2000. Ultrashort-pulse lasers: big payoffs in a flash. Sci. Am. 283, 72–79.

Joseph, D.D., Preziosi, L., 1989. Heat waves. Rev. Mod. Phys. 61, 41–73.

Joseph, D.D., Preziosi, L., 1990. Addendum to the paper on heat waves. Rev. Mod. Phys. 62, 375–391.

Kaganov, M.I., Lifshitz, I.M., Tanatarov, M.V., 1957. Relaxation between electrons and crystalline lattices. Sov. Phys. JETP 4, 173–178.

Kittle, C., 1967. Introduction to Solid State Physics. John Wiles & Sons, New York.

Meyers, M.A.., 1994. Dynamic Behavior of Materials. John Wiles & Sons, New York.

Momma, C., Chichkov, B.N., Nolte, S., von Alvensleben, F., Tunnermann, A., Welling, H., Wellegehausen, B., 1996. Short-pulse laser ablation of solid targets. Opt. Commun. 129, 134–142.

Nicholas, T., Recht, R.F., 1990. Introduction to impact phenomena. In: Zukas, J.A (Ed.), High Velocity Impact Dynamics. John Wiley & Sons, New York, pp. 1–63.

Özisik, M.N., Tzou, D.Y., 1994. On the wave theory in heat conduction. ASME J. Heat Transfer 116, 526–535.

Perry, M.D., Staurt, B.C., Banks, P.S., Feit, M.D., Yanovsky, V., Rubenchik, A.M., 1999. Ultrashort-pulse laser machining of dielectric materials. J. Appl. Phys. 85, 6803–6810.

Qiu, T.Q., Tien, C.L., 1992. Short-pulse laser heating on metals. Int. J. Heat Mass Transfer 35, 719–726.

Qiu, T.Q., Tien, C.L., 1993. Heat transfer mechanisms during short-pulse laser heating of Metals. ASME J. Heat Transfer 115, 835–841.

Shirk, M.D., Molian, P.A., 1998. A review of ultrashort pulsed laser ablation of materials. J. Laser Appl. 10, 18–28.

Touloukian, Y.S., Powell, R.W., Ho, C.Y., Klemens, P.G., 1970. In: Thermal Conductivity, Thermophysical Properties of Matter, vol. 1.

Touloukian, Y.S., Buyco, E.H., 1970. In: Specific Heat, Thermophysical Properties of Matter, vol. 4. IFI/Plenum, New York.

Trent, H.M., Stone, D.E., Beraubien, L.A., 1972. Elastic constants, hardness, strength, elastic, limits, and diffusion coefficients of solids. In: Gray, D.E. (Ed.), American Institute of Physics Handbook. McGraw-Hill, New York, pp. 2–60.

Tzou, D.Y., 1992. Thermal shock phenomena under high-rate response in solids. In: Tien, C.L. (Ed.), Annual Review of Heat Transfer IV. Hemisphere, Washington, DC, pp. 111–185 (Chapter 3).

Tzou, D.Y., 1995a. A unified field approach for heat conduction from micro- to macro-scales. ASME J. Heat Transfer 117, 8–16.

Tzou, D.Y., 1995b. The generalized lagging response in small-scale and high-rate heating. Int. J. Heat Mass Transfer 38, 3231–3240.

Tzou, D.Y., 1997. Macro- to Microscale Heat Transfer: The Lagging Behavior. Taylor & Francis, Washington, DC.

Wang, X.Y., Riffle, D.M., Lee, Y.S., Downer, M.C., 1994. Time-resolved electron-temperature measurement in a highly excited gold target using femtosecond thermionic emission. Phys. Rev. B 50, 8016–8019.

Wellershoff, S.S., Hohlfeld, J., Gudde, J., Matthias, E., 1999. The role of electron–phonon coupling in femtosecond laser damage of metals. Appl. Phys. A 69 (Suppl.), 99–107.